LOAN DOCUMENT

PHOTOGRAPH THIS SHEET

DTIC ACCESSION NUMBER

LEVEL

INVENTORY 0

RIA-81-2146

DOCUMENT IDENTIFICATION

27 Sep 79

"DTIC USERS ONLY"

DISTRIBUTION STATEMENT

HANDLE WITH CARE

ACCESSION FOR

NTIS GRA&I

DTIC TRAC

UNANNOUNCED

JUSTIFICATION

BY

DISTRIBUTION/

AVAILABILITY CODES

DISTRIBUTION	AVAILABILITY AND/OR SPECIAL
A-1	

DISTRIBUTION STAMP

DATE ACCESSIONED

DATE RETURNED

19990517031

19990517031

DATE RECEIVED IN DTIC

REGISTERED OR CERTIFIED NUMBER

PHOTOGRAPH THIS SHEET AND RETURN TO DTIC-FDAC

DTIC FORM 70A JUN 90

DOCUMENT PROCESSING SHEET

PREVIOUS EDITIONS MAY BE USED UNTIL STOCK IS EXHAUSTED.

LOAN DOCUMENT

TV

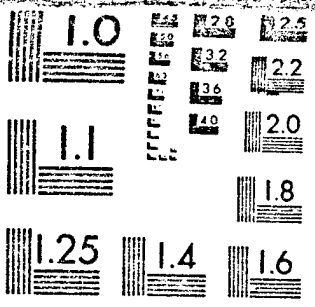

PREPRINT UCRL- 82756

CONF-790975--1

Lawrence Livermore Laboratory

MODELING ADDITIVE AND HOSTILE PARTICULATE INFLUENCES IN GUN COMBUSTION TURBULENT EROSION

A. C. Buckingham

September 27, 1979

This paper was prepared for the post print Proceedings of the 1979 CPIA-JANNAF Combustion Conference
U. S. Naval Postgraduate School, Monterey, California, September 10-14, 1979

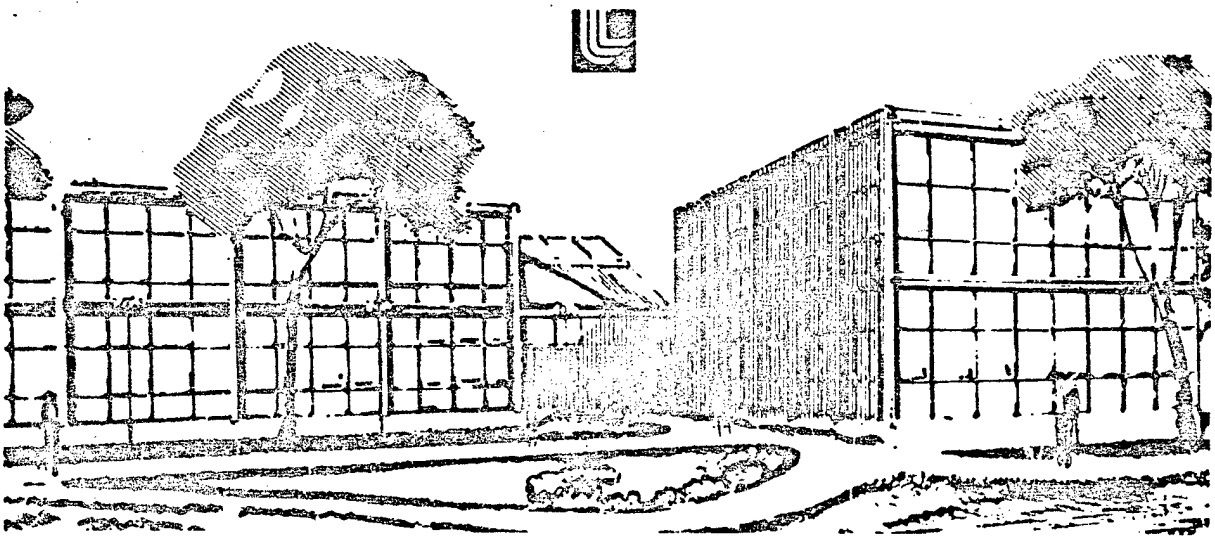

BLANK PAGE

MODELING ADDITIVE AND HOSTILE PARTICULATE INFLUENCES IN GUN COMBUSTION TURBULENT EROSION*+

A. C. Buckingham
University of California, Lawrence Livermore Laboratory
Livermore, California 94550

ABSTRACT

Research on fundamental mechanisms of erosion is the incentive for development and application of the numerical methods discussed here. The methods link particulate statistical dynamics to continuum turbulent reactive flow and solid material dynamic (erosive) surface response. The modeling incorporates calculated thermal, chemical, and mechanical dynamic processes in solid, liquid, gas, and mixed phases. The calculations match the multicomponent, turbulent, chemically-reactive wall boundary layer with the unsteady eroding interface boundary using microscopic transport, accommodation and energy distribution sub-models. Gas-borne particle motions are coupled to the turbulent flow in the inertial core and to the dissipative flow near the wall surface using two basically distinct numerical methods: (1) particulate turbulent gas flow, statistical dynamics and trajectory determination in the inertial core region; (2) solution of the detailed boundary layer heat and mass interface transport with boundary conditions and exchange properties modified for the unsteady influence of particle distributions and probabilistic surface dynamic response. Force, energy and motion coupling between particles and gas is assumed weak, with negligible back-influence from particles to gas flow structure. The present analysis is thereby restricted to relatively low mass loading which may be found in the ullage region between propellant bed and bounding walls, propellant face and projectile base as well as between propellant base and breech. Particle-to-gas relative fluctuational velocities are obtained at incremental time steps by numerical randomization. They are subject to the constraint that their ensemble averaged motions are, in sum, equivalent to the locally, apriori computed mean turbulent intensity. Results also include some preliminary molecular solid lattice statistical dynamics simulations. These address detailed estimation of the microscopic momentum and energy deposition and partition between a rapidly heated surface subjected to coincident particle collisions.

INTRODUCTION

Considerable attention has been paid to recently improved numerical simulations of gun barrel interior ballistics. Among these, promising detailed averaging techniques have been developed for computing two-phase flow,

*Work performed under the auspices of the U.S. Department of Energy by Lawrence Livermore Laboratory under contract #W-7405-Eng-48, and supported by the U.S. Army ARRADCOM Laboratories, Dover, N.J. and Aberdeen Proving Ground, Md. together with the U.S. Army Research Office (ARO), Durham, N.C. under contract #ARO 15812-MS.

+Approved for public release; distribution unlimited.

BLANK PAGE

stress, temperature and bulk thermochemistry that appear to dominate, at least in the large, the one-dimensional propellant bed combustion-convection and condensed phase motions, interior pressure development, and projectile accelerations.[1,2,3,4] Experimental correlation of some average predictions, particularly interior pressures and projectile motions, help to confirm the potential of these methods as tools for gun technology improvement.[5] Use of these promising results as a data base for developing initial and boundary conditions for subsequent detailed modeling of erosive flow, transport and wall material response appears reasonable and, to some extent, reassuring. Average dynamics, equation of state properties, burning rates, and bulk or volume averaged stress and temperature predictions are available for checking the consistency of detailed transport and kinetics calculations and predictions.

One of the considerations in propellant erosion studies is the influence of the populations of gas-borne particulates in the ullage regions surrounding the combusting propellant bed radially and the regions just ahead of and just behind the bed, Fig. 1. It seems intuitively reasonable that unburned (or burning) solid propellant particulates impinging on or abrasively sweeping the barrel walls will enhance wall erosion by augmenting heating and shear and exothermic gas-surface chemical processes (by continuous exposure of surface reaction sites). It has been observed, however, that erosion even in the presence of these "hostile" particulates can be countered to some extent by certain "benign" particulate additives which act in some, as yet, incompletely understood manner (momentum transport buffering?, thermal sinks?, thermal radiation buffers?, reduction of transport gradients?, paticulate cloud chemical absorption layers?, particulate Dufour influences?, turbulent energy and vorticity dissipation nuclei?).[6,7,8,9]

The mechanisms inherent in particulate augmentation of erosion and additive particulate erosion suppression are the central issues in our current theoretical analysis. We abstract the problem to one of determining solutions of the coupled particulate laden flow and transport in the ullage region between propellant bed and projectile. We further simplify initial and boundary conditions at a planar non-moving porous interface with flux, temperature and pressure histories imposed so as to be consistent with that predicted by two-phase NOVA code internal ballistics solutions.[3,4]

The gas phase turbulent field generated by such a propellant flow is modeled as that which would be initiated by a porous multiple jet plate turbulence generator[10] decaying axially as implied by the experiments and by a conceptually similar turbulent wake decay analysis.[11] The initial and boundary conditions of this idealized abstraction are summarized in Fig. 2.

PROCEDURE

MODEL FLOW CONDITIONS

In previous studies[12,13] emphasis was placed on numerically simulating the complete, multi-dimensional Navier-Stokes flow field in the wake of an accelerating projectile. However, for our current purposes, it is appealing

$$U(t) = \tilde{U}(t) + U''(t'')$$
$$t'' \ll t$$

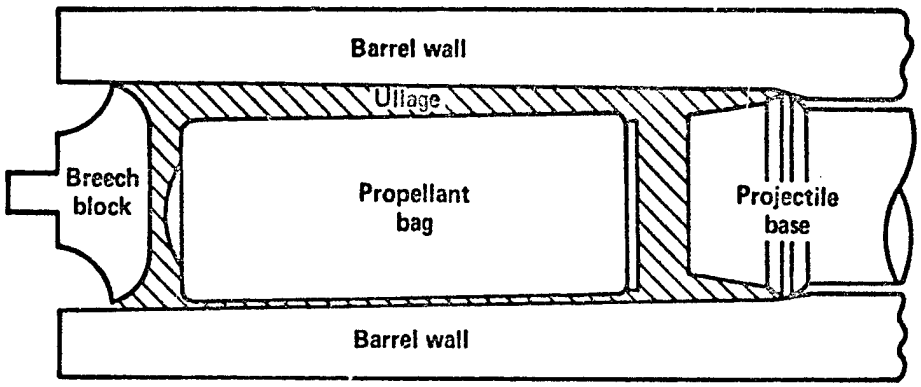

Fig. 1 Physical geometry of flow region examined.

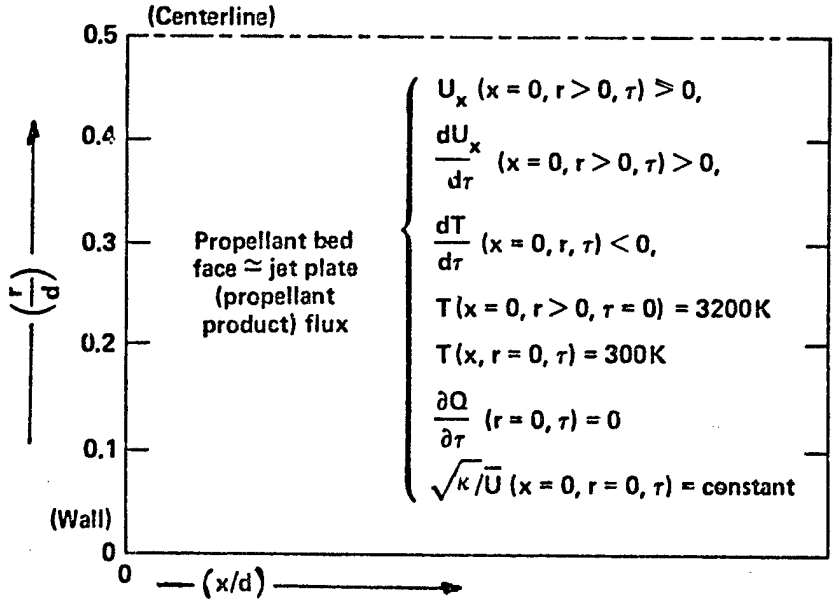

Fig. 2 Initial conditions for model problems.

to restrict our attention to details of the particle dispersal associated with an experimentally verified pure turbulent flow. Hence we remove consideration of the other complicating flow features associated with

accelerating projectile, projectile wake, and propellant bed combustion irregularities.[14]

The fluid dynamic situation which develops includes the solid aerosol consisting of sparse distributions of unburned propellants and erosion suppressive additives such as finely divided TiO_2, SiO_2, and talcum powder.

Particulate loading considered in the present analysis is that associated with sparse population densities of the order of 10^5 cm^{-3} or less. These relatively low mass loading levels together with characteristic aerosol size selected (0.1 μm to 10 μm) permit treatment of weak coupling from the carrier gas to the particle motions with neglect of back influence of the particles on the carrier gas. The original gun barrel situation is illustrated in Fig. 1 with decomposition of the flow into mean ($\bar{U}$) and fluctuating ($U'' = u^*$) components as noted. Our attention is on a simple conceptual region for the forward ullage region (shown cross-hatched) at early times. Boundary and initial conditions, shown in Fig. 2 include an accelerating inertial mean axial flow (U_x), a gradual cooling of the accelerating propellant products as implied by the time derivative of the interior temperature (T) from an initial flame temperature of 3200 K, the wall is initially cool (T = 300 K), entrance conditions are for a plane adiabatic duct (Q = heat flux) and the turbulence as represented by the kinetic energy (κ) at the jet plate origin is constant and homogeneous (immediately well-mixed).

CONTINUUM

The basic Navier-Stokes solutions subject to initial and boundary conditions previously described are obtained using: (1) a combination of the explicit MacCormack differencing scheme together with the two equation model closure of Wilcox and Traci and (2) the Briley-McDonald factored implicit scheme with a Jones-Launder two equation closure model. These produce the Navier-Stokes field quantities, together with turbulence kinetic energy, κ, and dissipation rate, ε.[12,13]

Mass conservation considerations for turbulent flow require global continuity, eq. (1), as well as both scalar time averaging, eq. (2) and vector velocity mass averaging, eq. (3). In the boundary layer region, gas phase, gas-surface, and surface chemical reactions require additional species conservation and production ($\psi_e \neq 0$) as well as multicomponent species diffusive exchange considerations, eq. (4).

Global

$$\frac{\partial \bar{\rho}}{\partial t} + \frac{\partial}{\partial X_j}(\bar{\rho}\tilde{U}_j) = 0, \text{ assumption } \frac{n_p m_p \langle U_p \rangle}{n_g m_g \langle U_g \rangle} \ll 1 \qquad (1)$$

time-averaged expanded sums:

$$\phi(t) = \rho, p, \tau_{ij}, q_j \ldots \quad \bar{\phi}(t) = \phi_f(t) + \phi_p(t) - \phi_g'(t), \qquad (2)$$

$$\bar{\phi}(t_0) \equiv \frac{1}{2\Delta t}\int_{t_0-\Delta t}^{t_0+\Delta t} \phi(t)\,dt \quad \text{and} \quad \bar{\phi}'(t) \equiv 0.$$

mass-averaged expanded sums:

$$\Phi(t) \rightarrow U_i, H, h, I \quad \tilde{\Phi}(t) = \Phi_g(t) + \Phi_p(t) - \Phi_g''(t) ,$$

$$\tilde{\Phi}(t_0) \equiv \frac{\overline{\rho(t_0)\,\Phi(t_0)}}{\bar{\rho}(t_0)} \text{ and } \overline{\rho\Phi''} = 0, \text{ but } \bar{\Phi}'' = \frac{\overline{\rho'\Phi''}}{\bar{\rho}} \neq 0 . \tag{3}$$

Species

$$\frac{\partial(\bar{\rho} m_\ell)}{\partial t} + \frac{\partial}{\partial X_j}(\bar{\rho}\tilde{U}_j m_\ell) - \frac{\partial}{\partial X_j}\left[\bar{\rho} D_\ell^T \frac{\partial m_\ell}{\partial X_j} - j_\ell\right] = \psi_\ell , \tag{4}$$

$D_\ell^T = D_\ell(\text{Molec}) + D_\ell(\text{Turb})$; ψ_ℓ (Net production rate of ℓ specie).

Substitution of the velocity perturbations in the compressible Navier-Stokes equations, scalar averaging (eq. (2)) and mass averaging (eq. (3)) and applying global continuity (eq. (1)) results in the compressible Reynolds equation for time-averaged momentum,

Momentum

$$\frac{\partial(\bar{\rho}\tilde{U}_i)}{\partial t} + \frac{\partial}{\partial X_j}\left[\bar{\rho}\tilde{U}_j\tilde{U}_i + \Theta\delta_{ij}p - \Theta\left(\bar{\tau}_{ij} - \overline{\rho U_i'' U_j''}\right)\right] = 0 , \tag{5}$$

$$\Theta \equiv \frac{v_g}{v_g + v_p} . \tag{6}$$

In addition to the Reynolds' stress term, $\overline{\rho U_i'' U_j''} = R_{ij}$, eq. (5) introduces void fraction weighting, defined by eq. (6), and developed by writing, separately, the equations for particle motions and gas phase motions, then combining them through simplified force and condensed phase production (weak coupling) considerations to form the mixture representation, eq. (5). To complete the weak coupling between turbulent field and the particle field requires that an explicit evaluation must be made of the forces on the particles induced by the turbulent motions. This will be addressed subsequently. At this stage one may note that the stress terms in the elementary mixture balance equation are simply weighted by the void fraction. The weighting gives the correct vapor phase limit as the relative volume occupied by the particles becomes negligible ($V_p/V_g \approx 0$) and implies, correctly, as discussed by Crowe[14], that for light particle mass loading the particles contribute negligibly to the mixture stress tensor. The coupling is weak. There is, as anticipated, no back influence develops from the particles to the mixture.

In terms of the total enthalpy, H (the sum of internal energy, pressure work, and mean flow kinetic energy) the corresponding energy equation for the turbulent mixture of particles and vapor is,

Energy

$$\frac{\partial(\bar{\rho}\tilde{H}-\bar{p})}{\partial t}+\frac{\partial}{\partial X_j}\left[\bar{\rho}\tilde{U}_j\tilde{H}+\Theta\bar{q}_j+\overline{\Theta\rho U_j''h''}-\Theta\tilde{U}_i\left(\bar{\tau}_{ij}-\overline{\rho U_i''U_j''}\right)-\Theta\overline{U_i''\left(\tau_{ij}-\frac{\rho U_i''U_j''}{2}\right)}\right]$$

$$-\frac{\partial}{\partial X_j}\left[\sum_{\ell}\left(\bar{\rho}D_\ell^T\frac{\partial m_\ell}{\partial X_j}-j_\ell\right)\tilde{h}_\ell-\frac{R\bar{T}}{\rho}\sum_{\ell}\sum_{m}\frac{\alpha_m D_\ell^T}{M_\ell D_{\ell m}}\left(\frac{j_\ell}{m_\ell}-\frac{j_m}{m_m}\right)\right]=0\ . \tag{7}$$

The third (bracketed) divergence term on the species mass and flux gradients is added in the reacting boundary layer region only. The core flow is assumed a mixture in thermo-chemical equilibrium and is described in conservation balance by the sum of the first two terms, consistent with Crowe's formulation.[14]

Closure of the system of equations (1), (5), and (7) requires an equation of state developed so as to be consistent with the NOVA code predictions.[3,4,5] In addition, closure relationships for the mean Reynolds stress, R_{ij} must be supplied. We assume a constitutive relationship, eq. (8) which introduces two additional unknowns: κ (the specific turbulent kinetic energy) and e_T (the turbulent kinematic eddy viscosity). The eddy viscosity is related to the turbulent kinetic energy and <u>one</u> additional unknown quantity: either the turbulent energy dissipation rate (ε) or the mass-weighted pseudo-vorticity ($\tilde{\omega}$) as seen in eq. (9). To solve for either of these two systems, the Launder-Spalding[12,13] differential closure relations are invoked, eqs. (10a) and (11a) or the Saffman-Wilcox-Traci[12,13] differential closure relations are invoked, eqs. (10b) and (11b). The closure relations obtained are substantially similar in form being of the convective-diffusive form with production based on interaction with the mean flow through the strain rate tensor, $\bar{S}_{ij}$. Turbulent correlations associated with fluctuations other than the fluctuating components of velocity (concentration, temperature, ...) are modeled at the present level with constant exchange coefficients, N^*_f eq. (12), specified at the initiation of a calculation.

$$R_{ij}=2/3\,\langle\rho\rangle\kappa-2\langle\rho\rangle e_T\left\{\bar{S}_{ij}-1/3\,\frac{\partial\langle U_k\rangle}{\partial X_k}\,\delta_{jk}\right\}\ , \tag{8}$$

$$e_T\equiv c_1\langle\rho\rangle\kappa^2\varepsilon^{-1}\equiv\langle\rho\rangle\langle\rho\kappa\rangle\tilde{\omega}^{-1}\ , \tag{9}$$

$$\left\{\frac{D\langle\rho\kappa\rangle}{Dt}=\frac{\partial}{\partial X_i}\left(\frac{e_T}{N^*_{\rho\kappa}}\frac{\partial\kappa}{\partial X_i}\right)+2e_T\frac{\partial\langle U_i\rangle}{\partial X_j}\bar{S}_{ij}-C_2\frac{\langle\rho\rangle^2\kappa^2}{e_T}\right., \tag{10a}$$

$$\left\{\frac{D\langle\rho\varepsilon\rangle}{Dt}=\frac{\partial}{\partial X_i}\left(\frac{e_T}{N^*_{\rho\varepsilon}}\frac{\partial\varepsilon}{\partial X_i}\right)+2c_2c_3\langle\rho\rangle\frac{\partial\langle U_i\rangle}{\partial X_j}\bar{S}_{ij}-c_4\langle\rho\rangle\frac{\varepsilon^2}{\kappa}\right., \tag{11a}$$

$$\uparrow\ \underline{\text{(Or)}}\ \downarrow$$

$$\left\{\frac{D\langle\rho\kappa\rangle}{Dt}\right]=\left[\alpha^*\langle\rho\rangle\bar{S}_{ij}-\beta^*\tilde{\omega}\right]\kappa-\xi^*\langle\rho\kappa\rangle\frac{\partial\langle U_k\rangle}{\partial X_k}\ ,\ \Bigg], \tag{10b}$$

$$\left\{\frac{D\langle\rho\tilde{\omega}^2\rangle}{Dt}=\left[\alpha^*\langle\rho\rangle\bar{S}_{ij}+\left\{\beta+2\sigma\left(\frac{\partial\ell}{\partial X_k}\right)^2\tilde{\omega}\right]\tilde{\omega}^2+\frac{\partial}{\partial X_j}\left[\mu+\sigma\langle\rho\rangle e_T\frac{\partial\tilde{\omega}^2}{\partial X_j}\right]\right., \tag{11b}$$

$$N^*_{pf} \equiv \sigma_T \frac{\partial \langle f \rangle}{\partial X_j} \cdot \left\{ \langle (\rho u_j)' f' \rangle \right\}^{-1} . \qquad (12)$$

Figure 3 illustrates the results of the continuum turbulent Navier Stokes solutions showing qualitative comparison between the calculated results and Klingenberg's[15] experiment in bore measurements. Figure 4 illustrates a similar quantitative comparison for the temperature field. Both flow calculations are taken from earlier results which include complicating features such as the projectile turbulent wake.[12,13] These vortical interaction features have been purposely omitted from our current analyses which use the simplified grid plate induced wind tunnel turbulence to isolate particulate turbulent coupling and transport.[16] Radial distributions of the time dependent turbulent intensity are illustrated in Fig. 5 and compared to the quasi-steady jet mixing experiments of Owen.[17] The Jones-Launder (J-L) model closure relations appeared to give qualitatively closer agreement to the experiments than did the Saffman-Wilcox-Traci (S-W-T) results. The Owen results are not appropriate for comparison with the near centerline predictions, since the experimental set-up used an isolated round jet as opposed to the homogeneous multiple

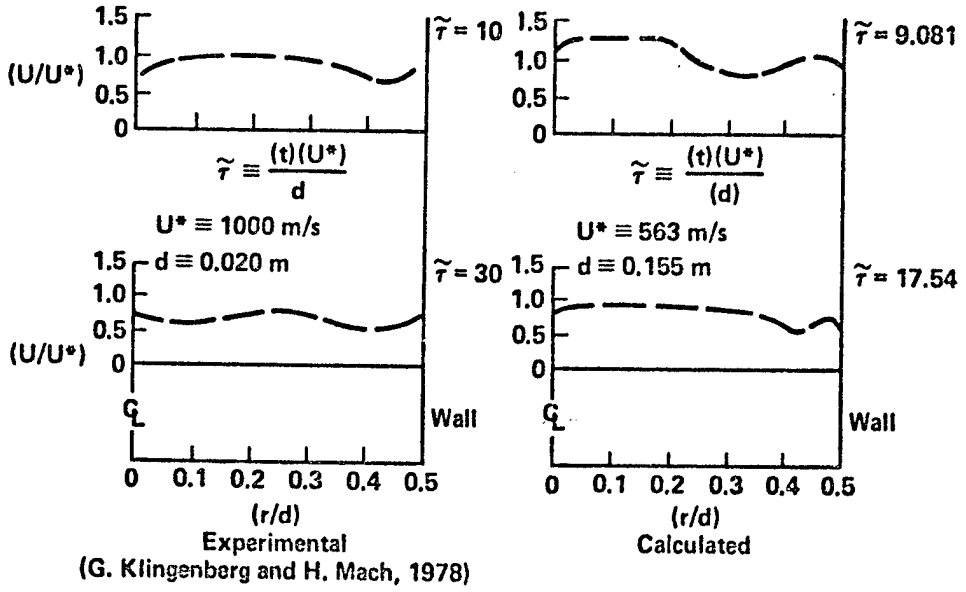

Fig. 3 Comparison of predicted and experimental velocity profiles.

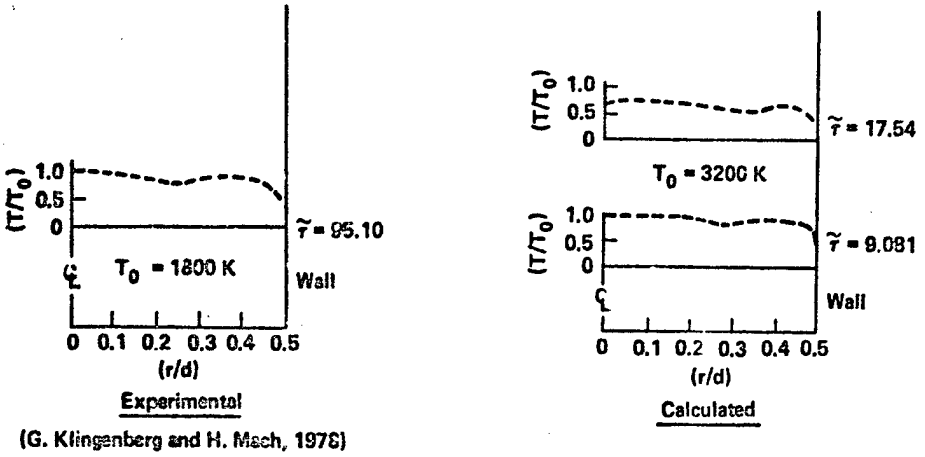

Fig. 4 Comparison of predicted and experimental temperature profiles.

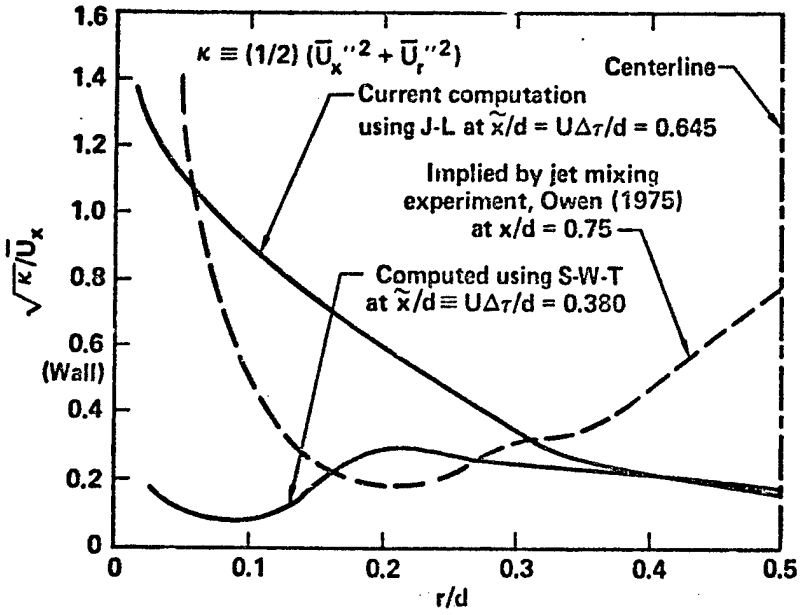

Fig. 5 Radial turbulent intensity profiles.

jet mixing region found near the turbulent grid plate. For comparison, the core and near centerline distributions the Betchov-Lorenzen[10] centerline axial distributions from their experiments were plotted against our theoretical predictions. Good agreement is found at several axial positions (measured from the grid plate origin in the downstream direction). These comparisons were reported in an earlier summary.[16]

BOUNDARY LAYER MATCHING

The wall boundary region is dominated by the steepest fluid-thermodynamic gradients yet its extent is small in comparison to the overall bore dimensions. In the current approach the multi-component reactive turbulent boundary layer solutions with wall ablation, recession, blowing and melt erosion are obtained by applying a separate non-similar, reactive boundary layer method. Boundary conditions are supplied by the core flow continuum solutions, together with the computed statistical particle concentration and energy distributions.[12] The matching of the separate computational domains, each with its own distinct formulation and method counters the numerical difficulties induced by the disparate time and length scales associated with each region. The solutions for Navier-Stokes reacting core flow and boundary layer flow are asymptotically matched in their overlap domain. Figure 6 illustrates the matching procedure. For "level" 2 additional conditions are needed and found. These require minimization of and together with the wake flow velocity and thermodynamic edge conditions to locate the wall boundary layer/core interface.[12,13] The matching procedure depends on the singular perturbation nature of the core generated turbulent region as the "outer solution" (the circled "e" region) in relation to the wall generated turbulent region as the "inner solution" (the circled "w" region). the overlap region to which the asymptotic matching is applied is shown cross-hatched.

The other matching "levels" shown in Fig. 6 include level (1) the ordinary (first order) boundary layer to core potential flow matching and level (3) which invokes an explicitly computed large scale turbulence structure, U_e'', as well as the small scale, U_e''', modeled as a continuum. Level (3) represents a subsequent step in the modeling which has not yet been completed.

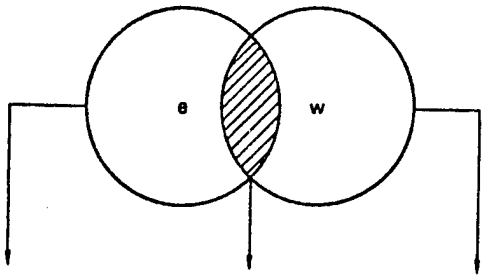

1)	$U_e = \tilde{U}_e$ $(R_{ij})_e \approx 0$	$\kappa, \epsilon, f' \to 0$ $\Delta s\, y_w \to y_e$	$(R_{ij})_w = F(\kappa, \epsilon, \tilde{U}_e)$
2)	$U_e = \tilde{U}_e + U_e''$ $(R_{ij})_e = F(U_e'') \neq 0$ $\langle U_e \rangle = \tilde{U}_e$	$[\kappa', \epsilon', f'] \to 0$ as $y_w \to y_e$	$(R_{ij})_w = F(\kappa, \epsilon, \tilde{U}_e, (R_{ij})_e)$
3)	$U_e = \tilde{U}_e + U_e'' + U_e'''$ $(R_{ij})_e^* = F(U_e'', U_e''')$ $\langle U_e \rangle = \tilde{U}_e + U_e''$	$[\kappa', \epsilon', f'] \to 0$ as $y_w \to y_e$	$(R_{ij})_w = F(\kappa, \epsilon, \tilde{U}_e, U_e'', (R_{ij})_e^*)$

Fig. 6 Schematic of boundary layer-core overlap procedure.

STATISTICAL TURBULENT PARTICLE MOTIONS

A novel feature of the present numerical simulations is the coupling of an array of particles to the Reynolds averaged Navier-Stokes gas phase motions. The statistical probability distributions associated with predicted localized (space and time) turbulent kinetic energy and dissipation rate results are obtained by numerical random (Monte Carlo) sampling of the turbulent excursion velocities.[14] The random perturbational velocity distribution is subject to a constraint that the ensemble average must correspond to the separately generated continuum flow field prediction of local turbulent intensity.

Aerosol motions are treated incrementally in time, Δt, following selection of the excursion velocities from the distribution sampling. Particle forces are then computed dependent on these statistical excursion velocities. The particle forces derived by Crowe[14], are rewritten in a Lagrangian framework moving with the mean gas dynamic flow, $\tilde{U}_i$. Forces considered include drag, virtual mass, Basset, Magnus, and Saffman Lift, in order, as indicated by eq. (13). These forces drive the particles in linear motions over trajectories limited, automatically, by the smallest time increment between collisions. Aggregate incremental motions simulate particle dispersion, momenta, energy, and wall collisions. Hard sphere particle-particle collisions are prescribed for particle encounters in the computations.

$$
\begin{aligned}
\underline{F}_p = {} & \frac{\pi d^2}{8} C_D \rho_f |u_j^* - u_{p,j}| (u_j^* - u_{p,j}) + \\
& C_1 \rho_f \frac{\pi d^3}{6} \left(\frac{\partial u_j^*}{\partial t} - \frac{\partial u_{p,j}}{\partial t} \right) + \\
& 3/2\, d^3 \sqrt{\pi \rho_f \mu} \int_t^{t+\Delta t} \frac{\partial}{\partial t} (u_j^* - u_{p,j}) (t - t')^{-1/2} dt' + \\
& \epsilon_{ijk} \frac{\pi d^2}{8} \rho_f (u_j^* - u_{p,j}) \omega_k + \\
& C_2 \sqrt{\mu \rho_f}\, d^2 (u_j^* - u_{p,j}) \left| \frac{\partial u_j^*}{\partial X_1} \right| .
\end{aligned}
\tag{13}
$$

The random sampling is applied for 1100 particles with expectancies distributed among 110 bins. The random velocity at any point $\vec{r_0}$ is a sum of the sampled velocities, $\langle \delta u^* \rangle$ plus the auto-correlation to the original (t_o) velocity fluctuation for the "memory" of the turbulent eddy as it evolves over the sampling time interval, Δt. This is shown in eq. (14) together with a schematic representing the bin subdivision over the sampling interval ($\Delta \equiv \Delta t$). The base distribution is considered to be the

normal distribution, eq. (15). Selective bin weighting is applied using the "importance sampling" techniques developed in chemical physics applications to selectively sample the most interactive portions of the spectra, hence speed convergence without exhaustively large numbers of selections.[18] Trial weighting functions are listed in eq. (16). Best results for the present cases were achieved using the parabolic bin weighting, $w_1 = 2(1 - \bar{\delta}^2)$, which favors the population near the origin (t_0).

$$u^*(\vec{r}_0, t_0 + \Delta t) = u^*(\vec{r}_0, t_0)\, R^*_{uu}(\vec{r}_0, \Delta t) + \langle \delta u^* \rangle, \tag{14}$$

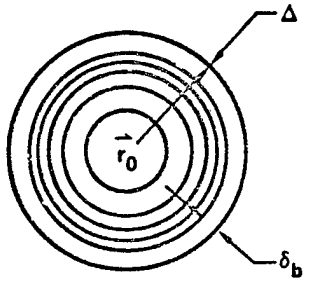

$$g(u - \tilde{u}) = (Y_{\delta u^*}\sqrt{2\pi})^{-1} \times \exp(-\delta u^{*2}/2Y^2_{\delta u^*}), \tag{15}$$

Bin weights:

$$w_l = \begin{cases} 1, \\ 3\bar{\delta}/2, \\ 1/2\bar{\delta}, \\ 3(1-\bar{\delta}), \\ 2(1-\bar{\delta}^2). \end{cases} \qquad \bar{\delta} \equiv \frac{\delta_b[l-1, l]}{\Delta}, \tag{16}$$

Specific emphasis of these calculations is on description of particle concentration size and mass distributions together with their resulting infuences on local flow composition, state and transport properties, as well as on gas-to-wall surface activity, energy and momentum transport.

Figure 7 shows the variance of the lateral dispersion about assumed centerline injection, predicted by the numerical simulations and applied to 0.3 μm and 5 μm aerosol particulates. The smaller particles relax with relative rapidity to the local turbulent flow motion so that their dispersal pattern almost matches that predicted by assuming an instantaneous equilibration to the local gas velocities. The larger particles, however, lag the local flow currents, creating narrower dispersion patterns and shortened penetration distances.

Figure 8 illustrates the effects of the initial particle distributions. From among the example packing distributions previously analyzed,[16] an initial packing conceptually arranged outside the flaps is selected as representative of one of the most effective configurations tested to achieve maximum dispersal of "benign" (erosion-suppression) additives. Size effects are evident in assessing the accumulated percentage of the original particle population reaching the wall.

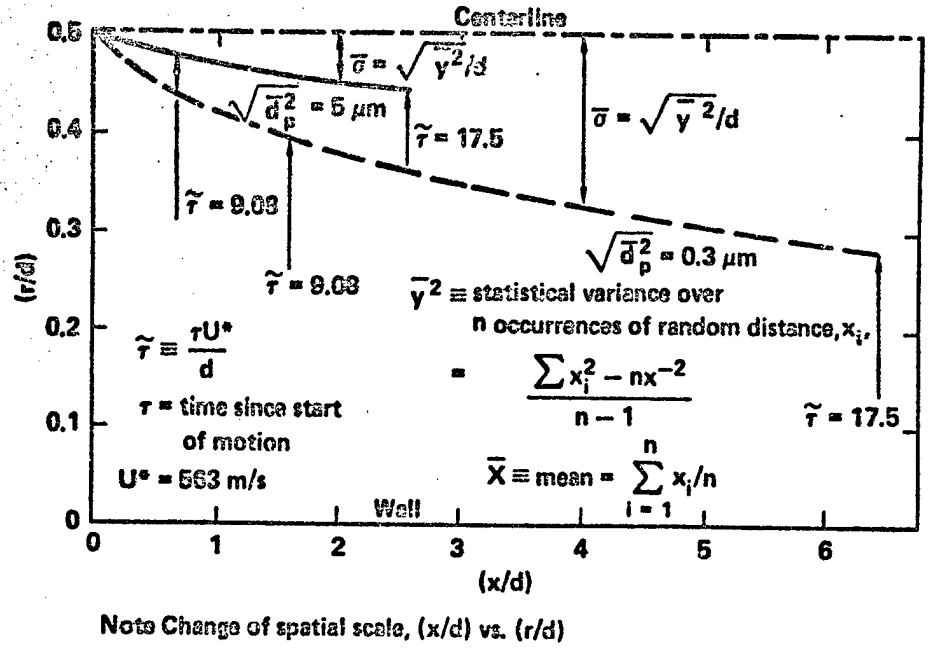

Fig. 7 Turbulent flow particle dispersal for centerline injection.

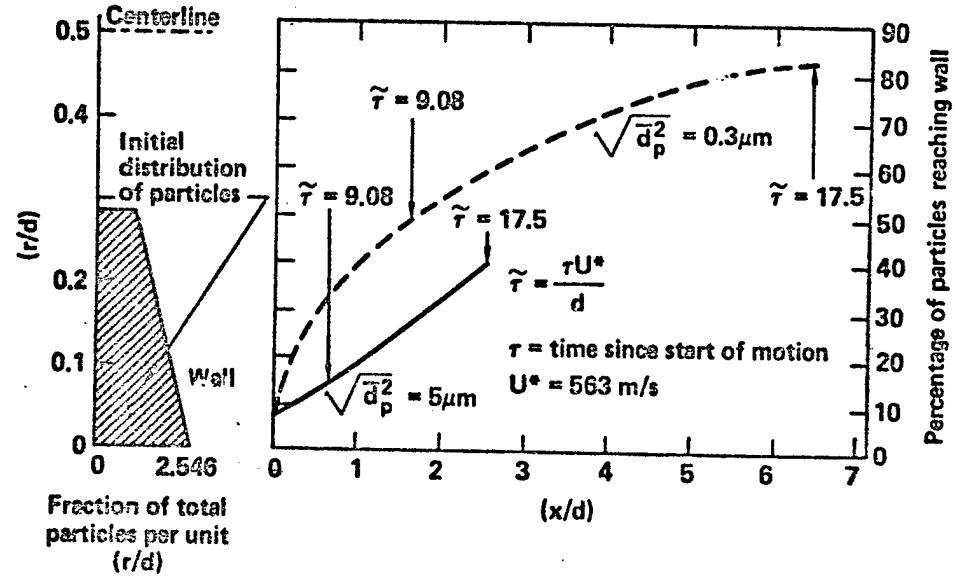

Fig. 8 Turbulent flow particle dispersal for indicated initial distribution.

BOUNDARY LAYER TRANSPORT AND WALL ACCOMMODATION

Additive particulate or "hostile" particulate concentrations are incorporated in the edge conditions through changes in the edge entropy profile, the corresponding gas state, and the altered conditions on the momentum integral due to increased mass flux. Within the boundary layer the transport exchange coefficients for multi-component species are adjusted with "frozen" contributions from the non-equilibrium thermal and momentum relaxation of the particles. Figure 9 shows the effects of two sizes of additive particles on boundary layer enthalpy profiles and on the wall shear. The indications are that twenty-five fold decrease in particle size corresponds to a 15% to 20% decrease in erosive wall heat, shear and mass transfer. In the absence of any particles the corresponding levels in erosive transport increase up to 40%.

A more detailed exposition of the particle influences on the transport processes, together with the theoretical perturbation method used to develop the particle-augmented gas transport properties is currently in preparation for a subsequent paper.[19] In addition, further illustrations of the effects of coincident wall surface micro-response and erosion on the transport processes will be provided in this subsequent paper. Here we will limit our discussion to some preliminary description of the modeling of additive laden gas to surface accommodation and energy partition.

The wall surface accommodation of energy and momentum associated with the arrival of the particulate cloud (a continuum distribution of particulates) can be modeled using a number of more or less successful engineering models on gas to surface transport. In the present analysis however, adoption of a particular modeled process, a priori, is self-defeating since the fundamental erosive mechanisms under investigation are imbedded in the model and its governing assumptions.

To circumvent overly-restrictive assumptions and to help unfold the fundamentals of gas-particulate-surface interaction, current use is made of molecular dynamics lattice collision calculations. These first principle, ab initio, molecular dynamics calculations are well-established procedures developed and refined by Karo, et al.[20] at Lawrence Livermore Laboratory to investigate details of kinetics, detonation, and combustion on a molecular level.

To supplement our knowledge of particulate laden gas surface energetics, Karo is applying this numerical statistical dynamic technique to the description of particulate collisions and energy deposition with modeled (brittle) wall surface layers of atoms simultaneously heated by boundary layer transport. To represent the thermally excited surface the lattice (a community of particles connected by modeled intermolecular potentials) is set into vibrational motions. Resonances induced by particulate collisions (the "particle" is another colliding lattice) are followed incrementally in time during the calculation. Energy deposition distributions, stress development and dynamics of lattice deformation which may signify failure are revealed as point defects (spall, dislocations, etc.) or as averages (in the ensemble sense) which may be extended to a macroscopic model of plastic deformation, failure and surface removal.

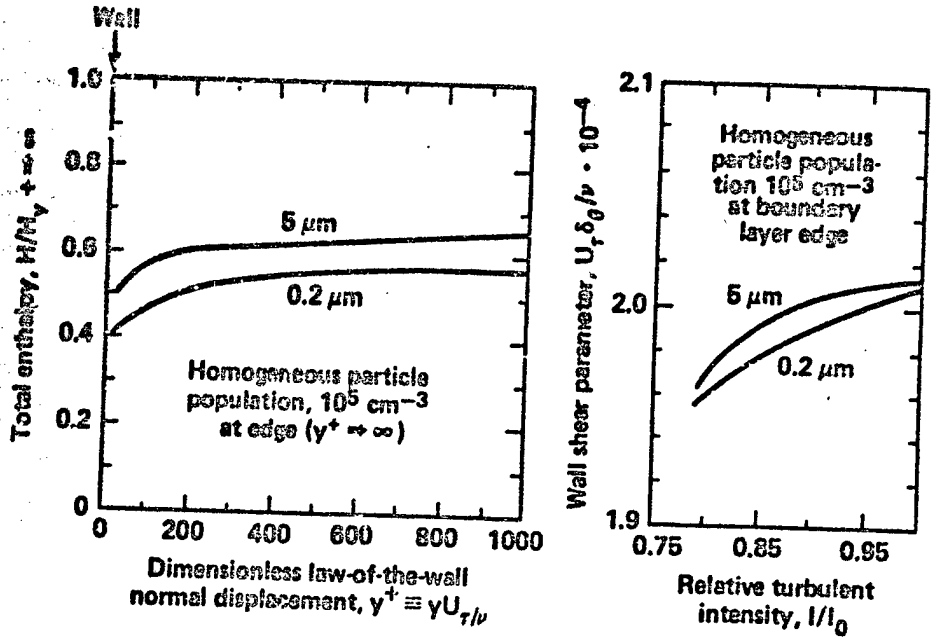

Fig. 9 Effects of particle size on near wall heating and shear.

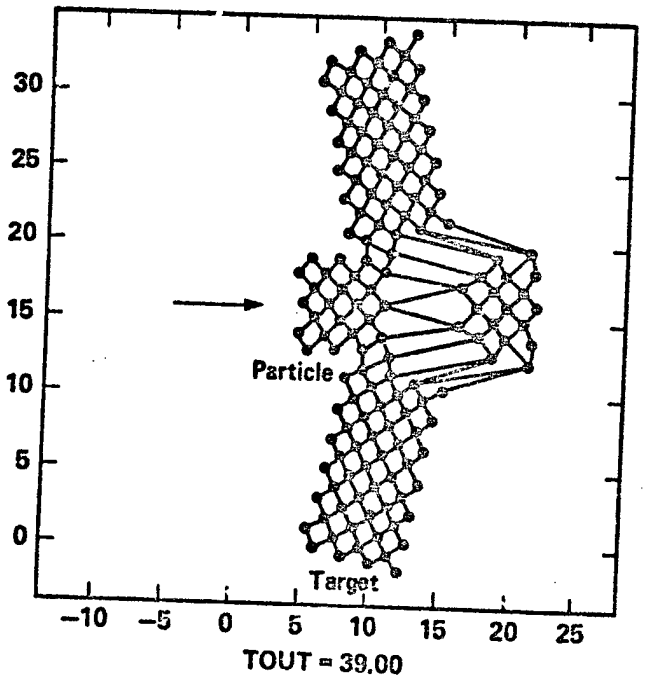

Fig. 10 Particle-wall lattice dynamics collision and heat transfer simulation.

Figure 10 is an illustration of an impact simulation showing the collision of a particle at the left hand side of a lattice group representing a surface layer of 8 molecules. The surface particle response to collision motions are frozen in the figure at a lattice-related characteristic frequency period of 39. The information generated by a systematic study of the time histories simulating a variety of such collisions and surface layer models are used to develop energy accommodation and partition information for the further development and modeling of erosive inducing transport mechanisms at the solid wall surface.

SUMMARY AND CONCLUSIONS

The present discussion emphasizes the matching of statistical mechanical and continuum modeled processes to help assess the role of particulates (both hostile and benign) on gun surface wall erosion. Particulate influences on erosion is offered here. The calculation and modeling at this time have emphasized:

- Effects of turbulence on species concentrations, thermal spatial distributions, and non-equilibrium relaxation of the particle field;
- Transport exchange influences of particulate clouds in the turbulent eroding wall boundary layer region;
- Modifications to properties for simultaneous heat, mass and particulate transfer, energy accommodation and partition on brittle surface layers based, in part, on gas-solid statistical dynamics considerations.

The primary (erosive-suppressive) influence of benign (non-burning) particles, if small enough to disperse rapidly with significant populations to the walls appears to be in:

- Mass-inertial and volumetric constraints act to reduce the molecular transport processes associated with the gas field;
- Particle flow in the boundary layer, comprising a moving curtain scatters incident particulates and fragments, preventing their reaching the wall;
- Particle curtain, associated with small diameter particles, offers considerably greater surface area than does the exposed wall; hence is an effective chemical absorption layer for hostile exothermic reactions, in addition it provides a scattering barrier for incident thermal radiation, effectively shielding the wall from these hostile influences;
- Particles in the core flow provide acoustical damping for the high frequency pressure oscillations which drive the fluctuating velocity field, hence act to damp (lower the intensity) of the combustion originated turbulence, and thereby lower the eddy transport of erosive heat and shear effects on wall erosion.

REFERENCES

1. Kuo, K. K., R. Vichnevetsky and M. Summerfield, "Theory of Flame Front Propagation in Porous Propellant Charges Under Confinement", AIAA Journ. (11), 444 (1973).

2. Kuo, K. K., "A Summary of the JANNAF Workshop on Theoretical Modeling and Experimental Measurements of the Combustion and Fluid Flow Processes in Gun Propellant Charges", Proc. 13th JANNAF Combustion Meeting (1976).

3. Gough, P. S., "The Influence of an Impact Representation of Internal Boundaries on the Ballistic Predictions of the Nova Code", Proc. of the 14th JANNAF Combustion Meeting (1977).

4. Gough, P. S. and F. J. Zwarts, "Modeling Heterogeneous Two-Phase Reacting Flow", AIAA Journ. (17), 17 (1979).

5. Horst, A. W., C. Nelson, and I. W. May, "Flame Spreading in Granular Propellant Beds", AIAA Paper 77-856, AIAA 10th Fluid and Plasma Dynamics Conference (1977).

6. Picard, J. P. and R. L. Trask, "Talc, A New Additive for Reducing Gun Barrel Erosion", Proc. Tri-Service Gun Propellant Symposium (1) (Picatinny Arsenal, Dover, N.J., October 1972) pp. 6.2-1 to 6.2-12.

7. Hasenman, H., "Review and Trends of Wear Reducing Additives in Large Calibre Tank and Artillery Cannon", Proc. of Interservice Technical Meeting on Gun Tube Erosion and Control (Watervliet Arsenal, Watervliet, New York, Feb. 1970) pp. 2.1-1 to 2.1-15.

8. Fedyna, R., M. E. Levy, L. Stiefel, "Use of Inorganic Wear Reducing Additives to Increase 7.62 mm Barrel Life with Single-Base Extruded Propellants", U.S. Army Research and Development Command Tech. Report ARSCD-TR-78004, Feb. (1979).

9. Russell, L. H., "Simplified Analysis of the Bore Surface Heat Transfer Reduction in Gun Barrels as Achieved by Using Wear-Reducing Additives", Naval Surface Weapons Center Report NSWC/DL TR-3378 October (1975).

10. Betchov, R. and C. Lorenzen, Phys. Fluids 17, 1503-1508 (1974).

11. Uberoi, M. S. and P. Freymuth, Phys. Fluids 13, 2205-2210 (1970).

12. Buckingham, A. C., "Propellant Driven Turbulent Interior Ballistics and Wall Erosion", U. of Calif. Lawrence Livermore Laboratory Rept. UCRL-81289 and AIAA Paper 79-0007, AIAA 17th Aerospace Sciences Meeting (New Orleans, LA, January 15-17, 1979).

13. Buckingham, A. C. and S. W. Kang, "Multi-Dimensional Interior Ballistics Computations on Wear and Erosion Mechanisms in Gun Barrels", in Proc. 1979 JANNAF Propulsion Meeting (Anaheim, Ca., March 6-8, 1979).

14. Crowe, C. T., "Vapor-Droplet Flow Equations", U. of Calif. Lawrence Livermore Laboratory Rept. UCRL-51877 (August 18, 1975).

15. Klingenberg, G. and H. Mach, "In-Bore Measurements of Gas Velocity and of Radial Gas Temperature Distributions", in Proc. Fourth International Symposium on Ballistics, sponsor, American Defense Preparedness Association (U. S. Naval Postgraduate School, Monterey, Ca., November 1978).

16. Buckingham, A. C., "Turbulent Dusty Gas Motions with Weak Statistical Coupling", AIAA Paper 79-1484, AIAA 12th Fluid and Plasma Dynamics Conference (Williamsburg, Va., July 23-25, 1979).

17. Owen, F. K., "Laser Velocimeter Measurements in Free and Confined Coaxial Jets with Recirculation", AIAA Paper 75-120 in AIAA 13th Aerospace Sciences Meeting (Pasadena, Ca., January 20-22, 1975).

18. Faist, M. B. and J. T. Muckerman, "Importance Sampling and Histogrammic Representations of Reactivity Functions and Product Distributions in Monte Carlo Quasiclassical Trajectory Calculations", J. Chem. Phys. 69, 9, 4087 (1978).

19. Buckingham, A. C., "Dusty Gas Influences on Transport in Turbulent Erosive Propellant Flow", to be presented in AIAA 18th Aerospace Sciences Meeting (Pasadena, Ca., January 14-16, 1980) and in Lawrence Livermore Laboratory Rept. UCRL-82876 (November, 1979).

20. Karo, A. M., J. R. Hardy, and F. E. Walker, "Theoretical Studies of Shock-Initiated Detonations", Acta Astronautica 5, 1041 (1978).

NOMENCLATURE

C_D	Modified Stokes drag coefficient on particles
d	Effective particle sphere diameter
$f_{p,i}$	ith component of particle force
$f_j(x_i)$	Probability density, frequency function in statistical weighting
$G(x_i,t)$	Integral average of a random property distribution
i_p	Particle internal energy
N	Number of samples in statistical average
T	Temperature

$\overline{U_j}$	jth component of mean velocity
u_j'	jth component velocity (fluctuation)
U_j	Total jth component velocity, sum of mean and fluctuating components
r_j	jth component vector distance
R_{ij}	Reynolds stress tensor
x_i	ith random variable in a turbulent field
ϵ	Turbulence dissipation rate
ϕ_j'	Arbitrary fluctuating component
κ	Turbulence kinetic energy
θ	Void fraction, ratio of gas volume to mixture volume
μ	Gas molecular viscosity coefficient
ρ	Gas density
ω_k	Particle rotational velocity component
V	Volume